REVIEWS

Journal of Semiconductors
(2021) 42, 013102
doi: 10.1088/1674-4926/42/1/013102

JOS

A review of *in situ* transmission electron microscopy study on the switching mechanism and packaging reliability in non-volatile memory

Xin Yang[1], Chen Luo[1], Xiyue Tian[1], Fang Liang[1], Yin Xia[1], Xinqian Chen[1], Chaolun Wang[1], Steve Xin Liang[2], Xing Wu[1,†], and Junhao Chu[1]

[1]Shanghai Key Laboratory of Multidimensional Information Processing, East China Normal University, Shanghai 200241, China

[2]Changjiang Electronics Integrated Circuit (Shaoxing) Co., Ltd, Shaoxing 312000, China

Abstract: Non-volatile memory (NVM) devices with non-volatility and low power consumption properties are important in the data storage field. The switching mechanism and packaging reliability issues in NVMs are of great research interest. The switching process in NVM devices accompanied by the evolution of microstructure and composition is fast and subtle. Transmission electron microscopy (TEM) with high spatial resolution and versatile external fields is widely used in analyzing the evolution of morphology, structures and chemical compositions at atomic scale. The various external stimuli, such as thermal, electrical, mechanical, optical and magnetic fields, provide a platform to probe and engineer NVM devices inside TEM in real-time. Such advanced technologies make it possible for an *in situ* and interactive manipulation of NVM devices without sacrificing the resolution. This technology facilitates the exploration of the intrinsic structure-switching mechanism of NVMs and the reliability issues in the memory package. In this review, the evolution of the functional layers in NVM devices characterized by the advanced *in situ* TEM technology is introduced, with intermetallic compounds forming and degradation process investigated. The principles and challenges of TEM technology on NVM device study are also discussed.

Key words: memory; transmission electron microscopy; *in situ* characterization; package; reliability

Citation: X Yang, C Luo, X Y Tian, F Liang, Y Xia, X Q Chen, C L Wang, S X Liang, X Wu, and J H Chu, A review of *in situ* transmission electron microscopy study on the switching mechanism and packaging reliability in non-volatile memory[J]. *J. Semicond.*, 2021, 42(1), 013102. https://doi.org/10.1088/1674-4926/42/1/013102

1. Introduction

In the post-Moore era, non-volatile memories (NVMs) have rapidly evolved from the scientific study to digital products, including mobile devices, electronic instruments and artificial intelligence[1–8]. The properties of non-volatility and fast operation speed make NVMs the main data storage devices[9–13]. The NVMs with feasible miniaturization and scalability are important for high-density storage. The typical NVMs include ferroelectric random-access memory (FeRAM)[14–16], resistive random-access memory (RRAM)[17–20], phase-change random-access memory (PCRAM)[21–23], floating gate random-access memory (FG RAM)[24–27] and magnetic random-access memory (MRAM)[28–30]. The high capacity and density storage performances are governed by different switching mechanisms of NVMs. Fig. 1 shows the historic trends and structural schematics of the above typical NVMs in SET and RESET conditions. The NVMs are being developed towards higher speed and smaller volume[11–13].

The NVM package structure is important to chip performance as well[31–37]. NVMs tend to work under the electrical field and the heating field. These external energies have a great effect on the atomic structure of devices, which brings changes in device performance. Many experiments concerning *in situ* electrical and heating stimuli have been performed. Also, more external stimuli experiments needed to be explored for further studies on the device performance[38–42].

The evolution of microstructure and composition could be characterized using transmission electron microscopy (TEM) in real-time. TEM is undoubtedly a powerful tool to study the switching mechanism in miniaturized NVMs at atomic scale[1–3]. This advanced technology was firstly demonstrated by Max Knoll and Ernst Ruska in 1931. In 1939, the first commercial TEM was produced. Since then, tremendous effort has been made to improve the spatial and energy resolution. The TEM machines with field-emission guns could offer a spatial resolution close to 0.1 nm under the acceleration voltages between 200 and 300 kV. Currently, the most advanced TEM with aberration correctors could reach a spatial resolution of 0.5 Å[1, 2]. The energy resolution of TEM also reaches 0.01 eV which could image various elements clearly. *In situ* technology could provide various external fields to investigate the performance of the device by using different TEM sample holders. The time resolution of *in situ* TEM is in milliseconds. The combination of TEM and *in situ* technology provides a workable solution to visualize the intrinsic structure-switching mechanism of NVMs and intermetallic compounds (IMCs) reliability issues in packaging. Nowadays, various external stimuli, such as electrical, heating, force, light and magnetic sample holders are used to investigate mechanisms in NVMs under a high vacuum chamber environment

Correspondence to: X Wu, Email: xwu@cee.ecnu.edu.cn
Received 26 APRIL 2020; Revised 4 AUGUST 2020.
©2021 Chinese Institute of Electronics

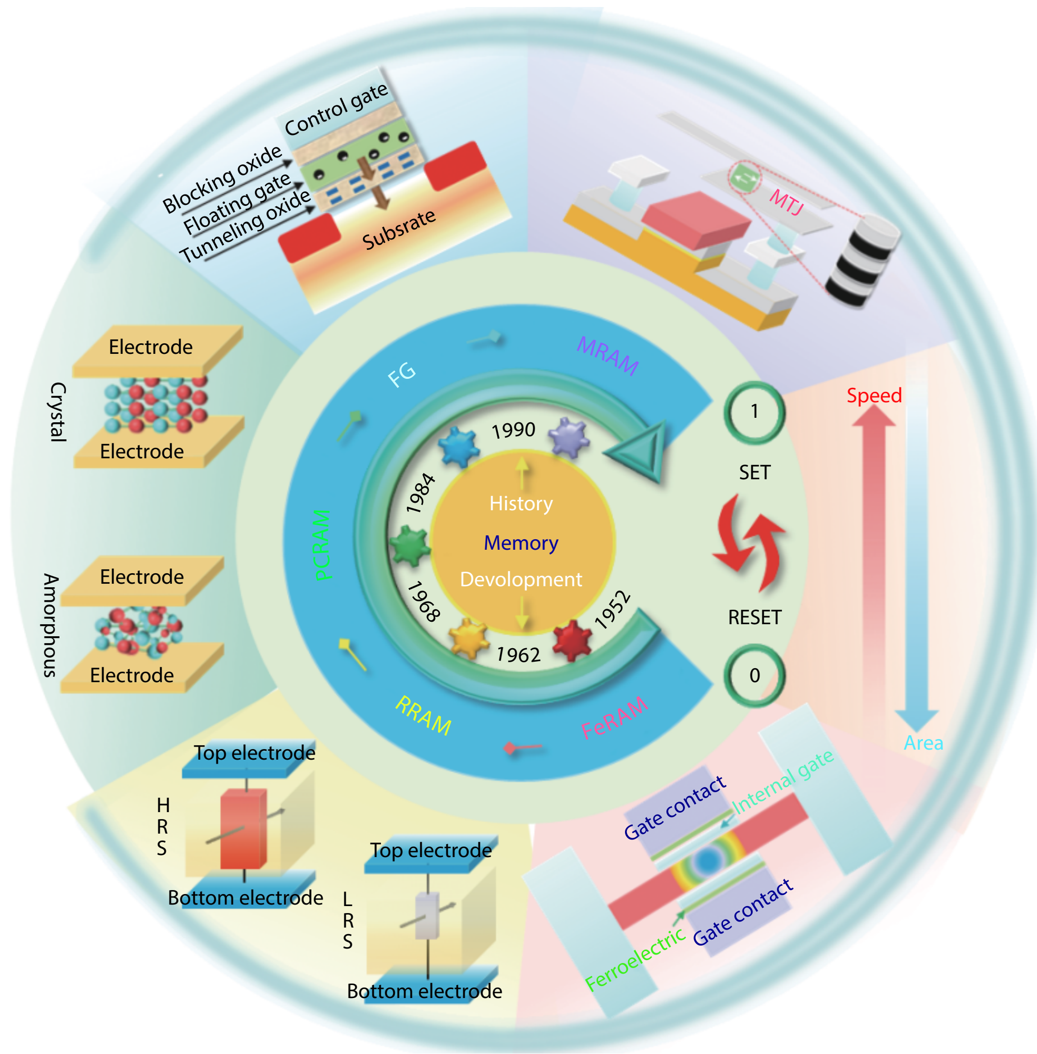

Fig. 1. (Color online) Advanced non-volatile memory devices.

without sacrificing the resolution[38–42]. As depicted in Fig. 2, with a variety of the *in situ* sample holders, the switching process could be dynamically monitored and manipulated under external stimuli simultaneously at the atomic scale[43–46]. The out circle represents different TEM holders that could perform *in situ* experiments. The sample holders ensure the external stimuli applied dynamically to realize various functions in the inner circle. In this review, we summarize the cutting-edge research on switching mechanisms of NVMs. The package reliability issue is also discussed. We primarily focus on *in situ* characterization techniques aiming to monitor and analyze the switching behavior of NVMs and IMCs at the atomic scale. Finally, a summary and outlook are provided for the bright future of the *in situ* TEM study in NVMs studies to improve device performance.

2. *In situ* study of non-volatile memories

2.1. Ferroelectric random-access memory

FeRAM is a promising non-volatile memory device for its low power consumption, fast work speed, and high reliability[16, 47–55]. The switching layer in FeRAM is the ferroelectric dielectric layer and the typical structure of FeRAM is depicted in Fig. 3(a). The ferroelectric materials have different polarization states under an external electrical field and Fig. 3(b) shows the corresponding structural diagram in the SET/RESET process. However, the switching mechanism is not clearly investigated by using traditional characterization tools. It is necessary to observe the microstructure changes directly. To understand the nature of switching states of FeRAM, a variety of *in situ* TEM experiments are performed[56–62].

One of the methods to observe polarization states of FeRAM is the diffraction technique. The Bragg diffraction condition changes, owing to different crystal orientations and structure, and the contrast of images changes accordingly. For example, a typical $BiFeO_3$ (BFO) film synthesized by standard solid-state reaction method consists of two phases: rhombohedral-like (R-like) phase and tetragonal-like (T-like) phase. The polarization of the two phases represents different resistance states with corresponding diffraction contrasts. Chiu *et al.* investigated the switching mechanism in BFO-based FeRAM and found that R-like and T-like structure transformed between each other during the SET/RESET process, as shown in Fig. 3(c)[56].

Generally speaking, the existence of defects and domain walls (DWs) could influence the device performance study. However, the microstructural changes of FeRAM during the switching process could not be observed directly by using the traditional characterization tools. In probing the effect of defects and DWs on the switching mechanism in FeRAM

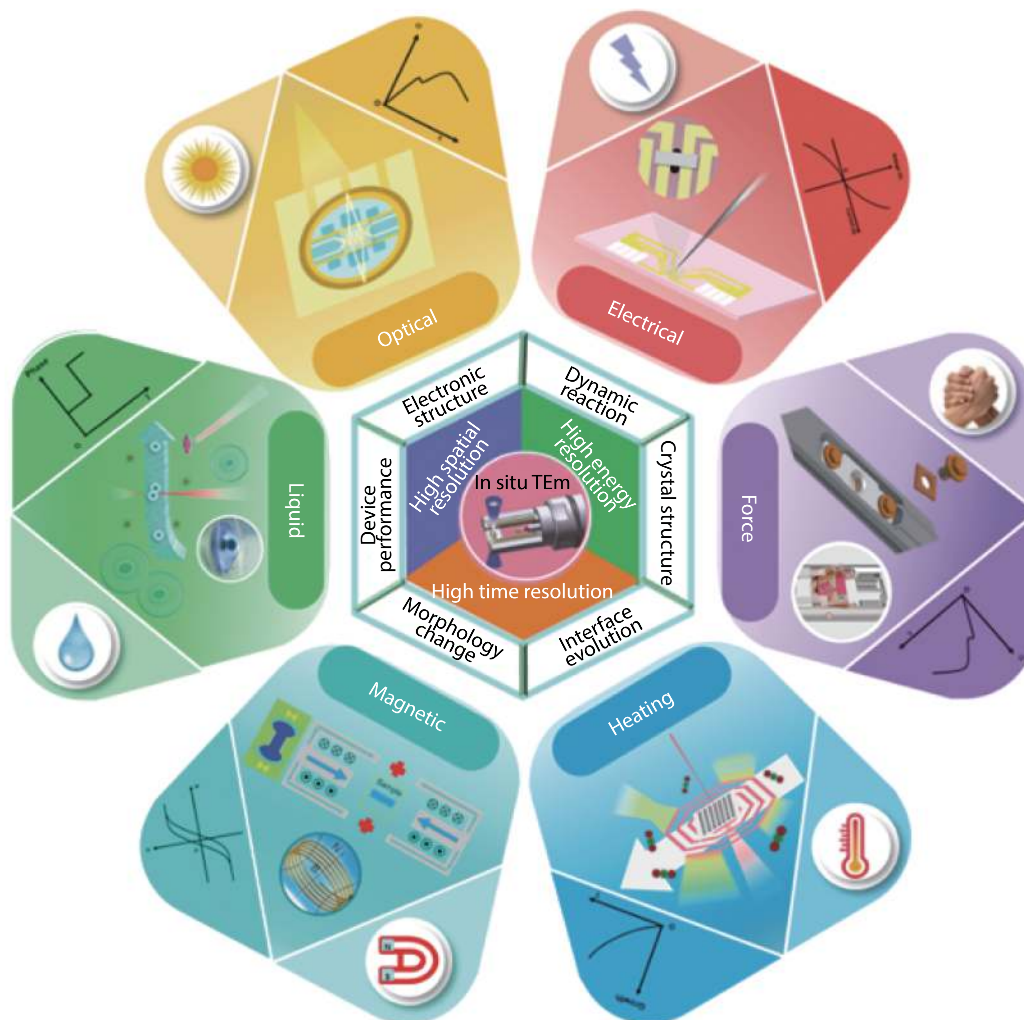

Fig. 2. (Color online) Overview of the *in situ* TEM characterization of memory devices in the wide range of external field stimuli, such as electrical, heating and magnetic fields.

device working conditions, the application of electrical field in TEM is necessary. Currently, the spatial resolution of TEM has reached 0.5 Å and the accuracy of current measured could reach 10^{-12} A[1]. Benefitting from the high spatial and current resolution, Li *et al.* characterized the atomic replacement during the switching process on the BFO-based FeRAM device by using the *in situ* electrical TEM[61]. It was found that defects could bring the polarization back-switching, which results in the data loss shown in Fig. 3(d). Direct observation of the DWs evolution in the BFO is obtained by Pan *et al.* under the *in situ* electrical field[57]. During the switching process, the free charge accumulated near the DWs and strong charge DWs (sCDWs) formed. It was found that sCDWs could improve the steady metallic conductivity of FeRAM through angle changes in DWs, as shown in Fig. 3(e). The generation and disappearance of sCDWs affect the resistance changes for the device switching process. The dynamics of polarization in SET/RESET has been shown in Figs. 3(f) and 3(g)[56, 61].

Besides BFO, studies have been carried out on the ferroelectric KH_2PO_4 materials as well. The perovskite-type material-ABO_3, such as $BaTiO_3$, $KNbO_3$, $LiNbO_3$ and PZT ($Pb(ZrTi)O_3$) become widely used[63]. Recent advances in atomic-level electron microscopy technology have made it possible to study high-quality FeRAM for its excellent work performance[64–67].

2.2. Resistive random-access memory

RRAM is a storage device that can switch between the low and high resistive states[19, 68–73]. A single memory unit is the metal–insulator–metal (MIM) structure with a dielectric layer sandwiched by a top electrode and a bottom electrode, as shown in Fig. 4(a). The switching behavior of the sandwich structure under a bias voltage was found by testing corresponding electrical characteristic curves. There are various explanations for the resistive phenomena in the MIM structure. Among these explanations, the widely accepted theoretical models are categorized into the interface resistance model and the filament conduction model. The interface resistance theory depends on the migration of oxygen atoms, and the filament conduction theory is based on the metal cations accumulation[73]. Fig. 4(b) depicts the schematic diagrams of the above two models. It is necessary to identify the structural changes in the two models[74–82]. To understand the nature of switching states of RRAM, a variety of *in situ* TEM experiments are performed for its high spatial and energy resolution for identifying the elements evolution during the switching process[83–87].

The main RRAM mechanism could be divided into vacancies and filaments, which are the nature of interface resist-

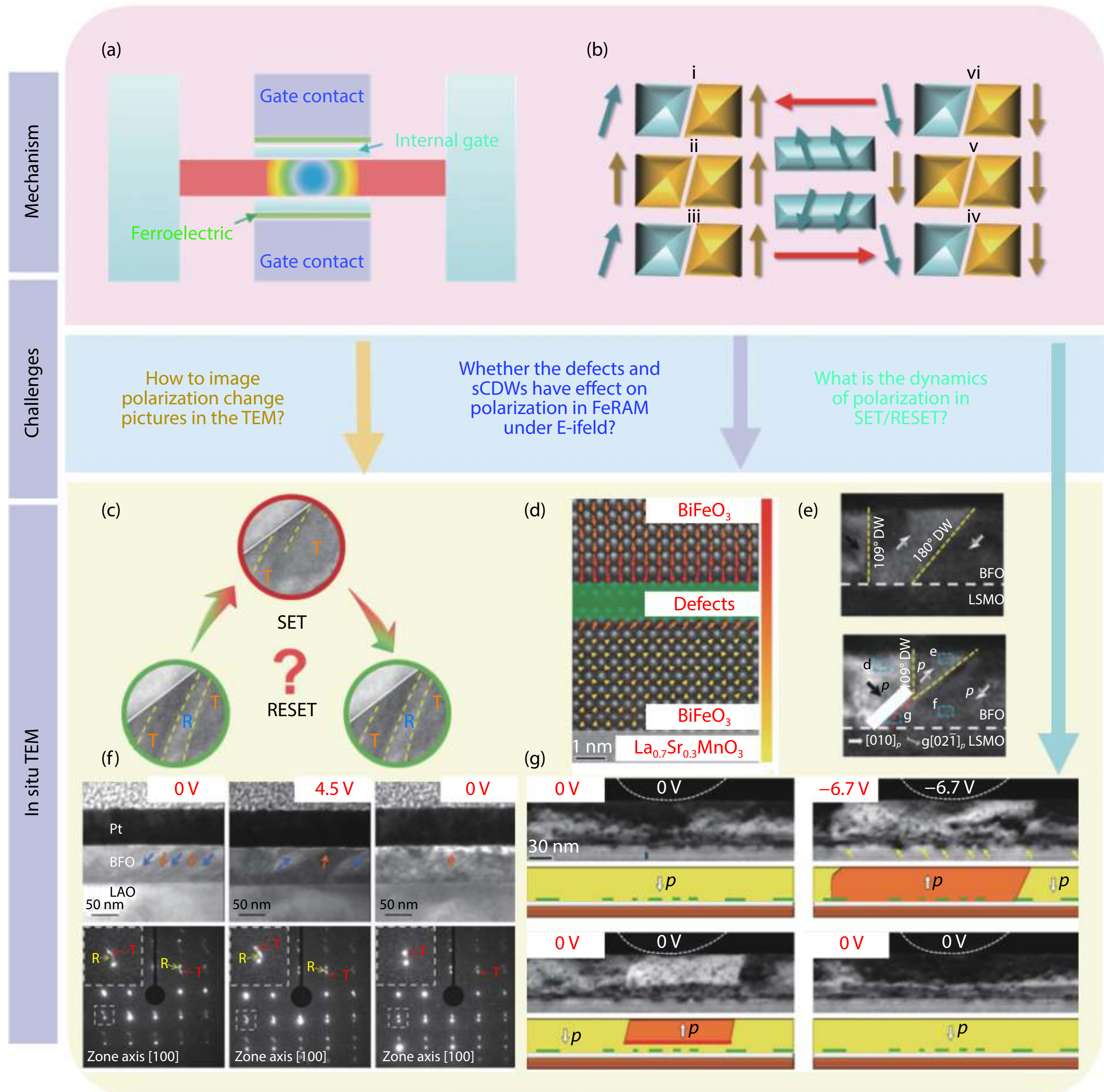

Fig. 3. (Color online) The switching mechanism of FeRAM and polarization evolution under the *in situ* environments. (a) Schematic of a typical FeRAM device. (b) Schematic diagram of polarization phenomenon in the SET/RESET process. (c) Structural changes of FeRAM during the switching of logic "0" and "1". (d) HAADF-STEM image of polarization mapping in a $BiFeO_3/La_{0.7}Sr_{0.3}MnO_3$ based-FeRAM device. (e) Cross-sectional dark-field TEM images with different DWs. The scale bar is 20 nm. (f) Cross-sectional TEM images and corresponding diffraction patterns of the ferroelectric materials under the *in situ* electrical biasing field in the phase transition process. (g) A series of TEM dark-field images about the evolution of an upward polarized domain to a downward polarized matrix.

ance theory and the filament conduction theory. The vacancies and filaments both participate in the formation of conduction filaments in RRAM in some cases[74, 75]. The Z-contrast technology based on high-angle annular dark-field (HAADF)-STEM theory is capable of imaging the filament contrasts owing to the differences of the atomic number. For example, the Ni filament could be directly characterized using Z-contrast depicted in Fig. 4(c). Electron energy-loss spectroscopy (EELS) technique could identify the chemical elements. Electrons undergoing inelastic scattering could be collected by the energy loss spectrum. For example, fewer oxygen atoms could be observed in the oxide when a conductive channel forms in the device shown in Fig. 4(d)[76].

The understanding of the dynamics of oxygen vacancies in RRAM is important to improve device performance. As shown in Fig. 4(d), the relationship between oxygen vacancies and high conductivity channel has been studied[76]. It was found that oxygen vacancies accumulated under an applied electric field. Then these oxygen vacancies had a chemical reaction with metal cations accompanied by changes in the valence bond. Finally, a conductive channel formed. Also, electrostatic force microscopy could detect the existence of oxygen vacancies as shown in Fig. 4(e). Notably, the accumulated charge remained stable after biasing suggesting that the charge corresponds to oxygen ions rather than electrons[88].

The relationship between metal filaments (MFs) formation/rupture and resistive switching process is important to enhance device performance, and the nature of its working principle deserves investigation. Theoretically, the conductive fila-

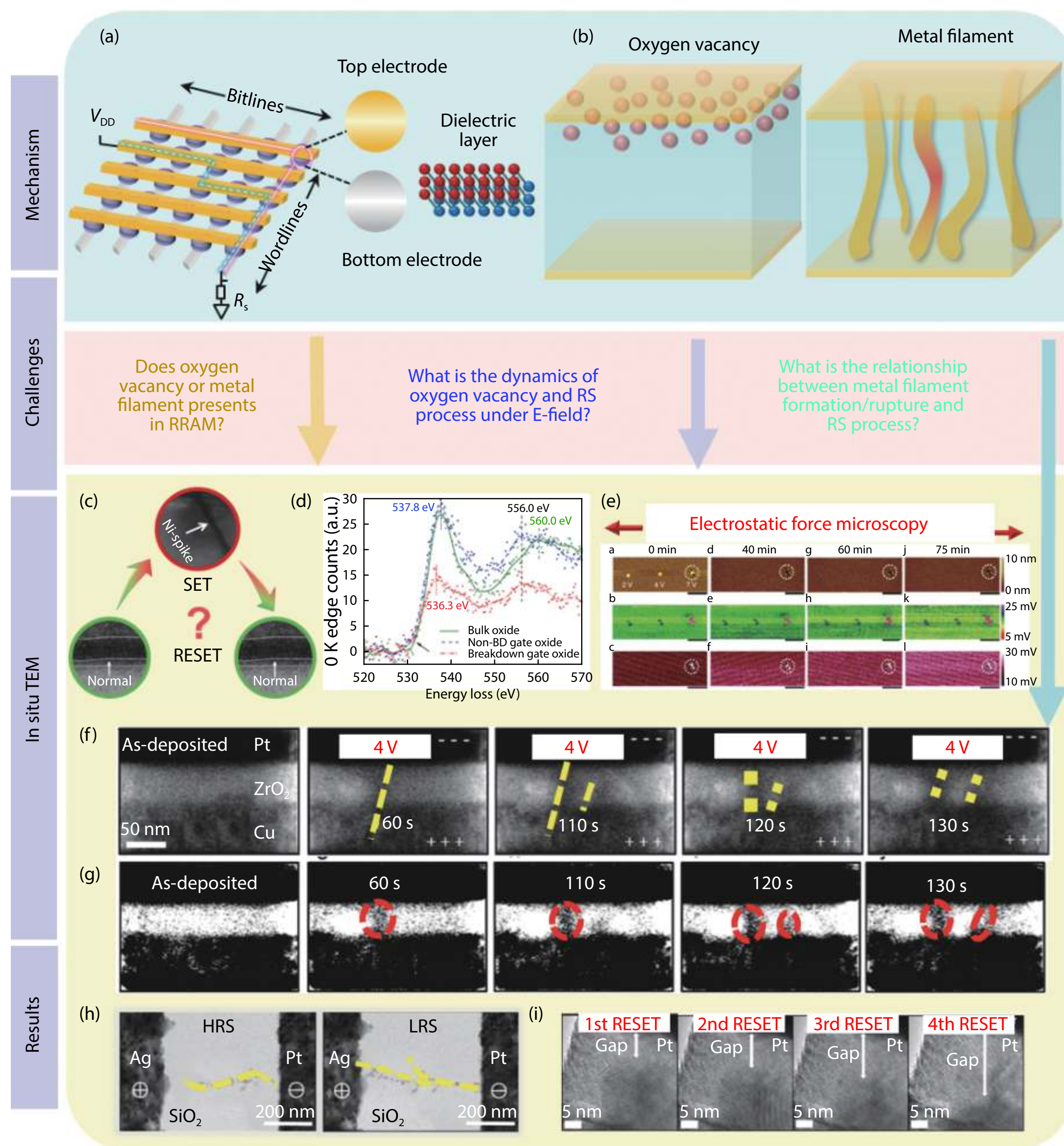

Fig. 4. (Color online) The switching mechanism of RRAM and interfacial evolution under the *in situ* environments. (a) Schematic of the RRAM array. (b) Schematic diagrams of oxygen vacancies and MF-based resistive switching models in the SET/RESET process. (c) Local structural changes of the functional layer in RRAM during the switching of logic "0" and "1". (d) The EELS oxygen K-edge spectra showing a lower oxygen count (more oxygen vacancies) in the device. (e) Topographic and electrostatic force microscopy results after removing the electrical stimuli suggesting that the charges observed should correspond to oxygen ions, instead of electrons. (f) A series of TEM images capturing the dynamic MF growth processes in the Cu/ZrO_2/Pt TEM device. (g) Black-and-white images converted from the raw TEM images of (f) to highlight the growth of MF. (h) TEM images symbolizing logic "0" and "1" in the RS process. (i) A series of high-magnification TEM images showing the dynamic dissolution process of the MF.

ment occurs in a local region at the nanoscale[62]. When a positive voltage is applied to the active electrode, the mobile active metal ions drift to the anode surface. The MFs will form after the accumulation of metal ions during the switching process. *In situ* electric testing is the most feasible method for investigating the MFs. Liu *et al.* did the pioneering work to directly observe the formation and rupture of MFs as shown in Fig. 4(f)[77]. Fig. 4(g) is the black-and-white images converted from the raw TEM images of Fig. 4(f) to highlight the growth of MFs. Also, Ag particles could be discontinuously distributed to form a conductive channel. When the distance between multiple filaments meets the hopping distance of electrons in the electric field, the channel can be formed, as shown in Fig. 4(h). The microstructure and dynamic dissolution process of the MFs can be characterized using high-resolution TEM imaging, as shown in Fig. 4(i)[77].

Various materials can be used in RRAM. For example, typical materials used in the active electrode are Ag, Ti and Al. $La_{0.67}Sr_{0.33}MnO_3$, $SrTiO_3$, TiO_2, ZrO_2, Ag_2S and Ta_2O_5 are commonly used materials for resistance material layer. Related research will be continuously promoted to improve the performance of RRAM[9] using *in situ* technology[89–96].

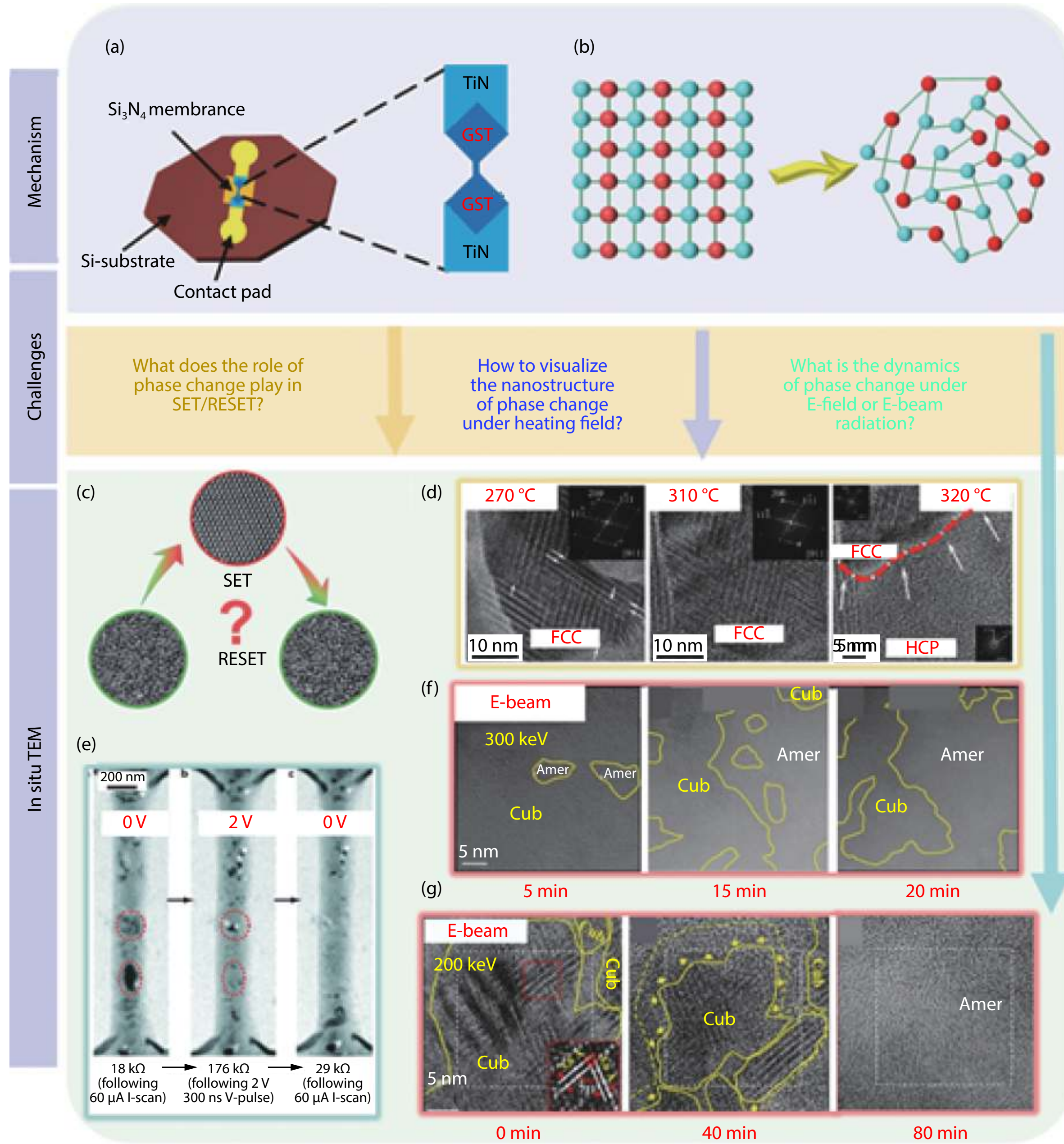

Fig. 5. (Color online) The switching mechanism of PCRAM and its nanostructure under the *in situ* environments. (a) Schematic of the PCRAM devices. (b) A schematic diagram of the phase change phenomenon occurs in the SET/RESET process. (c) The transformation between the crystal and amorphous phases in the memory devices from “0” to “1”. (d) A series of TEM images acquired during the *in situ* TEM heating field capturing the dynamic phase change process in the PCRAM device. The insets show the FFT patterns of the layer. (e) TEM images acquired showing the phase change under the *in situ* electrical biasing fields. (f, g) *In situ* amorphization of cubic GST at 300 °C with 200 keV e-beam irradiation, depicting the dynamic separation and shrinking of the cub-phase grains. The insets are the corresponding FFT patterns.

2.3. Phase change random-access memory

PCRAM with high integration and low power consumption is a promising NVM in the memory field. The construction of PCRAM is the MIM structure similar to the RRAM structure. The structure of PCRAM is shown in Fig. 5(a) and phase change in the dielectric layers are the core part[22, 97–103]. Phase change materials can transit between different phases with the corresponding resistance states displayed in Fig. 5(b). For example, Ge–Sb–Te (GST) exists in the two-phase change processes: from amorphous to face-centered cubic (FCC), and from FCC to hexagonal close packing (HCP). The GST exhibits semiconductor properties, semi-metallic properties, and metallic properties in the state of amorphous, FCC and HCP, respectively[104–106]. GST can transit from one phase to the other when applied to a critical voltage. A variety of *in situ* TEM experiments has been performed for the investigation on the nature of switching mechanisms in PCRAM[23, 107, 108].

With the development of electron microscopy, the role of phase change play in the SET/RESET process deserves an in-depth study. Phase-contrast plays an important role in characterizing crystal structure during the switching process. The phase-contrast depends on the multiple diffraction beam coherent imaging through the aperture of the objective lens. The phase-contrast is sensitive to crystal structure and fre-

quently used in the PCRAM studies as shown in Fig. 5(c).

The nanostructure changes during the switching process could be characterized directly by using *in situ* heating experiments. The heating sample holder is equipped with a micro-electro-mechanical system (MEMS) microheater by using a four-point probe that can measure the temperature changes. The temperature could reach a maximum of 1200 °C in a second without the sacrificing of atomic resolution. Fast Fourier transformation (FFT) is a method for the determination of phase structure. The interfacial spacing angle of the phase could be measured from FFT patterns to determine phase structure by comparing the data in the standard crystal library. For example, Lotnyk *et al.* performed *in situ* heating experiment on the GST sample. The FCC phase and HCP phase could be distinguished by the FFT method. It was found that the structure of the FCC phase is stable until the temperature increases up to 310 °C and transits to the stable GST HCP phase at the temperature of 320 °C shown in Fig. 5(d)[99].

Other *in situ* TEM technologies also play important roles in improving the performance of PCRAM, such as electrical field or e-beam radiation. Meister *et al.* used *in situ* electrical biasing fields to mimic the working environment[102]. It was found that the large crystalline phases disappeared during the electrical stressing as shown in Fig. 5(e). The structural changes brought resistance changes during the switching process. Also, the e-beam is a useful tool for the *in situ* manipulations of the crystal lattices to study the phase change. Jiang *et al.* studied the progressive amorphization of GST under the e-beam irradiation with different energies. The e-beam with higher energy leads to a more rapid amorphization process as shown in Figs. 5(f) and 5(g)[23].

Phase change materials used in PCRAM are developing. These materials could be categorized as: the binary alloy (GeTe), the ternary alloy (GeTeAs), and the multi-element alloy (AgInTeSb)[103–109]. These *in situ* images show that phase transition tends to occur through atomic displacement under external energy during the SET/RESET process. The dielectric layer phase changes could explain the above PCRAM instability by using the *in situ* TEM technology. To improve the performance of PCRAM, more advanced electron microscopy technologies and stable dielectric layer materials are needed[21, 110–117].

2.4. Floating gate random-access memory

Floating gate (FG) memory is important in the NVM market owing to the advantages of its high integration, high speed, low power consumption and good reliability. FG RAM is different from the previous memory devices. The charge could be stored in a floating gate layer[24–26, 118]. The schematic of the FG RAM devices is shown in Fig. 6(a), which has an extra capture layer compared to the traditional memory[118–124]. The extra capture layer between the gate and the substrate is to store the charge in the FG RAM. Based on the tunneling effect or hot electron injection effect, the charges pass through the capture layer for charging and discharging the floating gate. The specific charge movement process is shown in Fig. 6(b). However, the charge storage process could not be observed directly by using the traditional characterization tools. It is necessary to investigate the charge storage mechanism during the SET/RESET process. The electronic holography technique is used to directly observe charge storage.

Oxide materials with the high dielectric constant (κ) are widely used as the FG layer materials. The fabrication of the high κ layer is compatible with the semiconductor process. Li *et al.* investigated the oxygen vacancy-based conductive mechanism in the FG RAM in the HfO_2 film[123]. Oxygen vacancies in HfO_2 are induced when applied to a gate voltage as shown in Fig. 6(c).

The imaging technology based on the electric potential distribution is used to capture the distribution of oxygen vacancies. TEM equipped with electronic holography could visualize the electrical potential and morphology. The charge distribution could also be analyzed during the switching process. Fig. 6(d) displays the grain boundaries evolution due to the oxygen vacancies[125]. The accumulation of oxygen atoms could be observed in Fig. 6(e). The electric potential distribution is intuitively reflected by the e-beam phase distribution through the sample when the sample thickness is homogeneous. The electric potential distribution in the charge trapping layer under different gate bias is shown in Fig. 6(f).

How to link the charge distribution with the nanostructure of FGRAM is challenging. By taking advantage of the electrical potential and morphology, the charge distribution converted by the electric potential distribution could be obtained using the Poisson equation. This charge distribution has been further investigated[123]. As shown in Fig. 6(g), the charge distribution presents a non-uniform change with the increase of gate voltage values. The charge injected from some local places and reside there. This phenomenon could be explained by the non-uniform distribution of oxygen vacancies.

The traditional trapping layer materials are from SiO_2 to the high κ materials. Combining the electronic holography technique, the charge movement of charge trapping memory is revealed. It confirms that the positive gate voltage induces oxygen vacancies. More advanced technologies are needed for further studies[126].

2.5. Magnetic random-access memory

MRAM is a typical memory device with long work lifetime, high work speed, low energy consumption and high capacity density compared with the conventional DRAM[30, 127–132]. Fig. 7(a) shows the schematic of the MRAM devices[133–140]. The data in MRAM is not stored as a charge or current flow, but by magnetic domain changes. As is shown in Fig. 7(b), the directions of domain changes when applied a voltage depicted by different colors[141]. However, the dynamic changes of the magnetic domain could not be observed by using conventional technology. Energy loss magnetic chiral dichroism (EMCD) technology has been contributed to study the MRAM switching mechanism[127–132].

The domain changes are subtle and transient and it is difficult for directly characterization magnetic structure of complex magnetic materials in microscopic regions[142]. The present occupant technology to characterize domain changes is X-ray magnetic chiral dichroism (XMCD)[143–145]. The signal of XMCD is produced by the virtual photons. The XMCD technique can distinguish the magnetic order of anti-ferromagnetism and ferromagnetism, which provides a new way to detect magnetic signals of materials. However, the spatial resolution is not high, owing to the wavelength of X-ray.

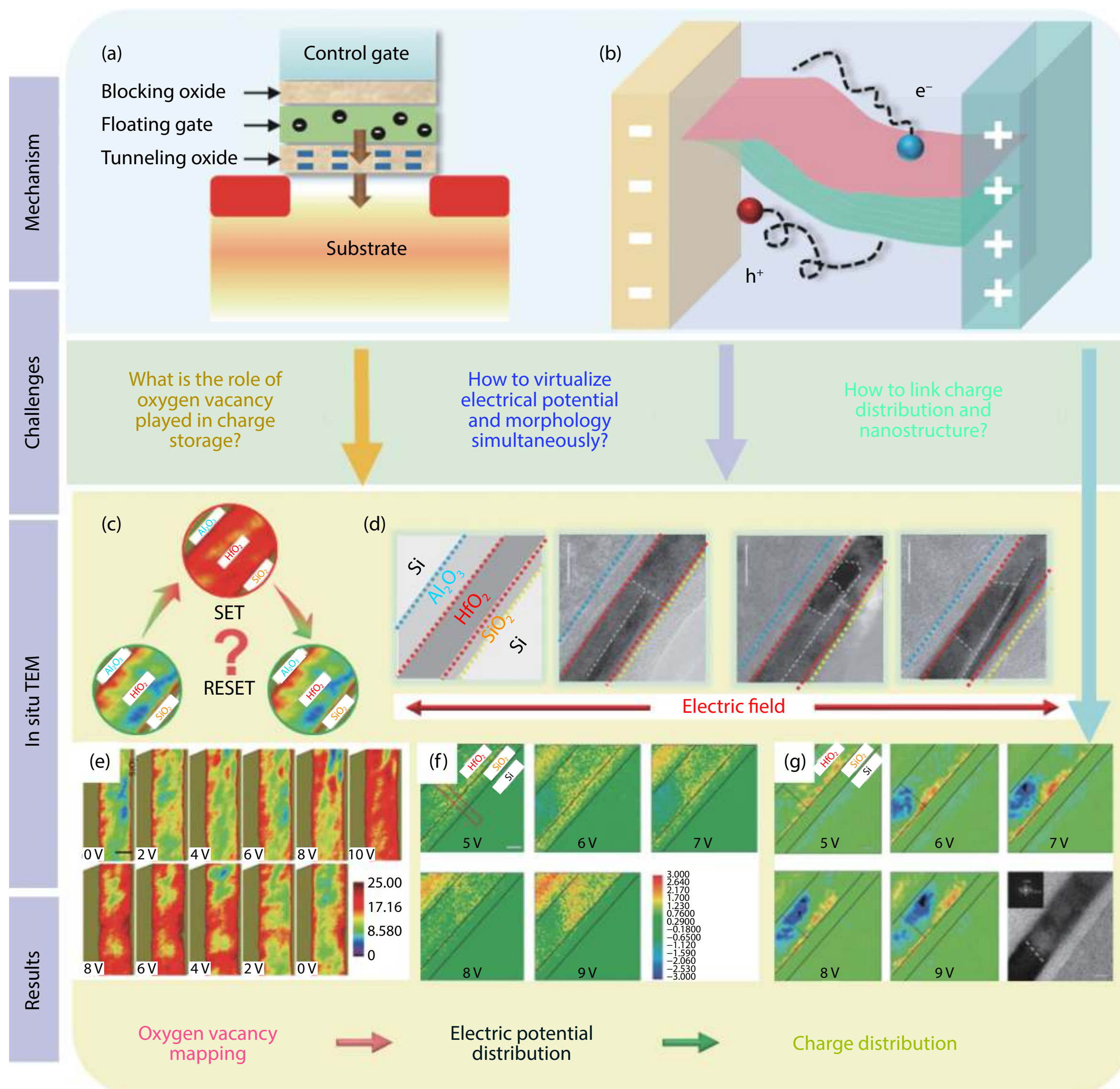

Fig. 6. (Color online) The switching mechanism of floating-gate RAM and its nanostructure under the *in situ* environments. (a) Schematic of a typical floating-gate RAM device. (b) Schematic diagram of the charge storage in the memory device. (c) The corresponding internal oxygen vacancies distribution as the FG RAM transit from “0” to “1”. (d) Structural diagram of FG memory and high-resolution TEM images of the HfO_2 capture layer. The white lines represent the position of grain boundaries. (e) A series of patterns concerning oxygen concentration in the trapping layer under the *in situ* electrical biasing fields. (f) Phase/potential mapping within the trapping layer at different biases. (g) Projected charge distribution at different biases in the trapping layer.

Therefore, EMCD technology was developed and its signal is collected along with the EELS signal. The EELS are detected using electron beams from specific apertures marked by yellow circles as shown in Fig. 7(c). Compared to XMCD, it can distinguish the spin magnetic moment from the orbital magnetic moment at the nanometer scale, which means higher spatial resolution. Vortex beam with orbital angular momentum could be obtained under the e-beam modulation for the EMCD experiments. By analyzing the differences in the EMCD spectrum, information on the magnetic properties of the atom could be obtained.

The principle of the EMCD to observe domain changes is the second challenge needed to be discussed to better understand EMCD technology. The corresponding equipment details are shown in Fig. 7(d)[142–145]. It is possible to distinguish the magnetic properties of a given element by examining the EMCD spectrum at its characteristic energy.

The dynamics of imaging magnetic domain changes under the e-beam is important. Wang *et al.* studied the magnetic material – Sr_2FeMoO_6 (SMFO) exhibiting different types of magnetic coupling[128]. As shown in Fig. 7(e), the experimental achromatic spatially resolved EELS (SREELS) image of the double perovskite SFMO is depicted. Combining with the chromatic aberration correction with SREELS, their work demonstrated the atomic-scale imaging of EMCD from the individual Fe/Mo-O (004) atomic planes in the double perovskite SFMO. Fig. 7(f) reveals the arrangements of all atoms in the SFMO along with the $[110]_{pc}$ zone axis by the negative spherical aberration imaging technique. The pattern with arrows is the normalized background-subtracted SREELS images recorded at the oxygen *K* edge. The vertical spacing of 2 Å in the SREELS image at the oxygen *K* edge is consistent with the interplanar spacing between adjacent Fe/Mo-O and Sr-O atomic planes. The atomic-scale image of EMCD could be achieved

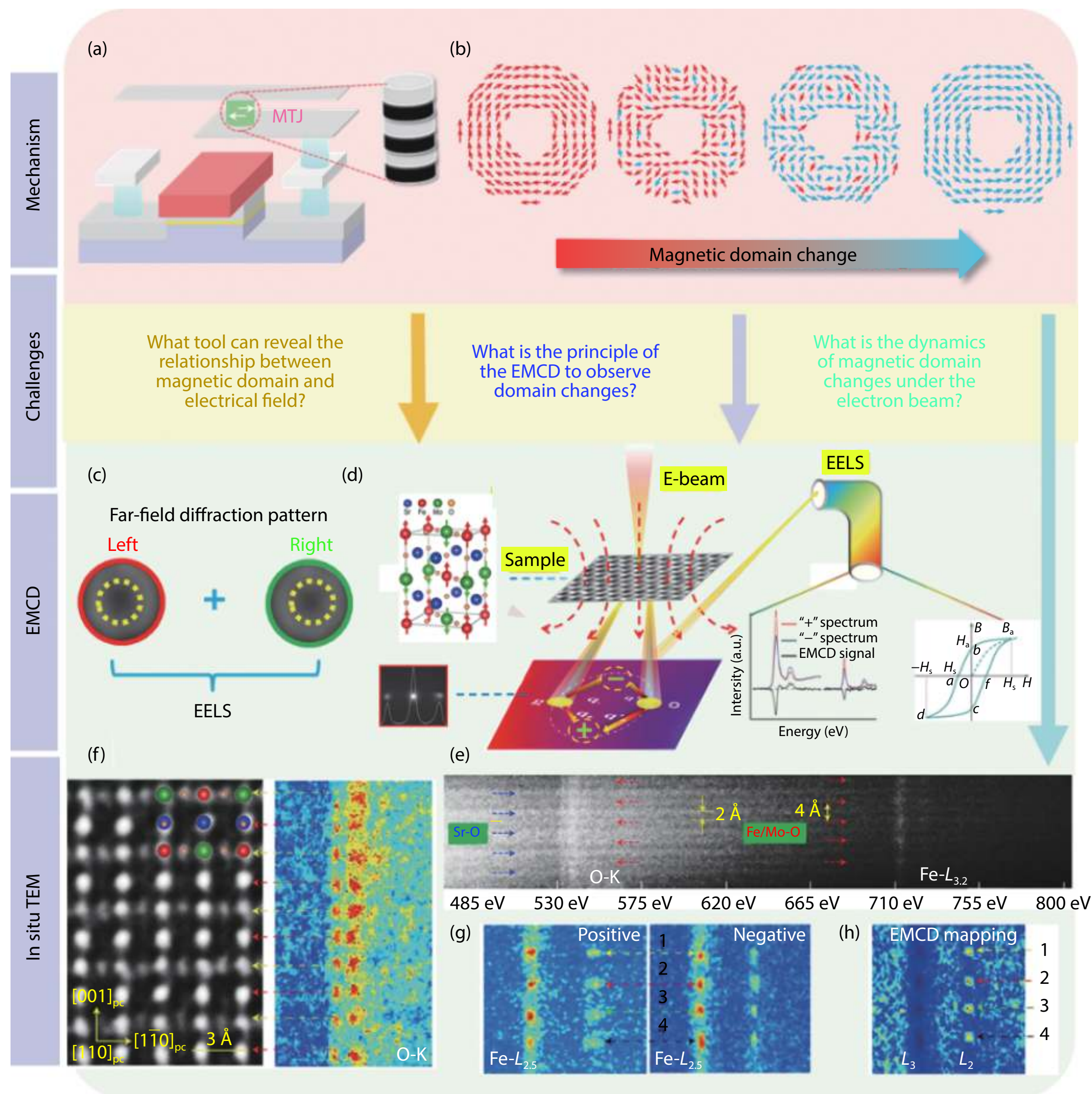

Fig. 7. (Color online) The switching mechanism of MRAM and its nanostructure by using advanced technology. (a) Schematic of the MRAM devices. (b) A schematic diagram of domain changes during the SET/RESET process. (c) Far-field diffraction pattern showing the different positions of the spectrometer entrance aperture for the left and right sidebands. Specific apertures are marked by yellow circles. (d) Schematic diagram of the EMCD technology working principle. (e) Raw achromatic SREELS image of the oxygen *K* edge and the Fe $L_{3,2}$ edge of the double perovskite Sr_2FeMoO_6 without using an objective aperture. (f) Negative spherical aberration imaging of Sr_2FeMoO_6 and the corresponding projected structure model before tilting the sample. The arrows represent normalized background-subtracted SREELS images recorded at the O *K* edge. (g) Normalized background-subtracted SREELS image depicting the Fe $L_{2,3}$ edge acquired at the '+' and '–' positions, respectively. (h) Atomic-scale image of EMCD achieved by subtracting the SREELS image acquired at the '+' position from that acquired at the '–' position.

by subtracting the SREELS images acquired at the '+' and '–' positions shown in Fig. 7(g). Fig. 7(h) shows the atomic-scale image of EMCD of SMFO from different SREELS images. The ratio of the spin to orbital magnetic moments could be obtained from the EMCD mapping to investigate the magnetism.

The EMCD technology is capable of understanding the physical origins of magnetic properties of materials at the highest spatial resolution. The principle of EMCD technology offers the possibility of achieving combined local atomic-scale magnetic, chemical and structural characterization. It is useful to promote technological development and improve device reliability in advanced MRAM technology[146–150].

3. *In situ* study of memory package

High integration density requires chip-level interconnection to ensure device performance. A high-quality memory package in NVMs is important for retaining the existing data under high working temperatures. The encapsulation diagram of the memory devices package is shown in Fig. 8(a). The pins of the circuit on the silicon chip are connected to the external joint with wires. This ultra-thin structure brings new challenges. The major one is the wire bonding (WB) lifetime under the high temperature. Intermetallic compound (IMC) formations between the two interfaces as-bonded conditions are critical for the WB lifetime, as shown in Fig. 8(b)[37].

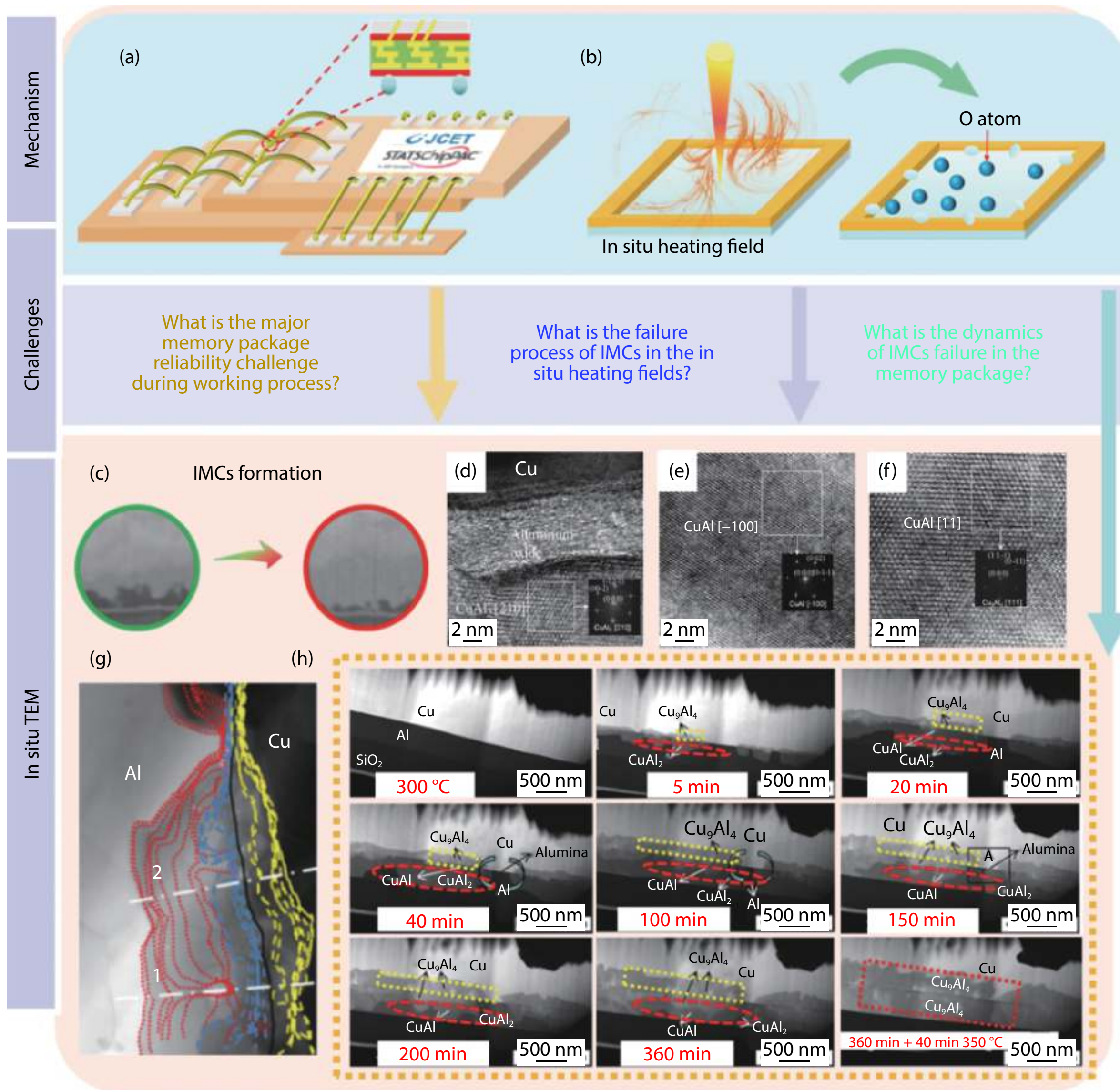

Fig. 8. (Color online) The WB reliability of memory package. (a) Encapsulation diagram of the memory devices package. (b) A schematic diagram of the bonding void formation in the annealing process. (c) Cross-section focus ion beam image of the Cu-Al interface. (d–f) Lattice images and Fourier reconstructed pattern of $CuAl_2$ (θ), CuAl (η_2) and Cu_9Al_4 (γ_2). (g) The STEM-BF image where the successive positions of the IMCs transformation interfaces, as indicated by the dashed lines. (h) Identification of sequential microstructure evolution of IMCs during the thermal annealing period under the *in situ* heating field.

It is difficult to find the failure area accurately at the nanoscale. However, combining TEM with various external field sample holders, it is possible to implement an *in situ* manipulation platform in TEM to observe the real-time evolution of materials[3].

WB stability is important for NVM device performance. Among different WB materials, a copper alloy or palladium coated copper (PCC) is used to replace the conventional copper to prohibit oxidation. The chemical reactions of IMC under the thermal field changes the alloy stoichiometric. As shown in Fig. 8(c), take Cu–Al IMC as an example, the aluminum oxide as the protection layer is broken down and new IMCs formed. Various patents are proposed to improve performance such as the “integrated passive stacking for RFICs and MEMS in a system-in-package” by Liang *et al.*[151]. The patent provides a high level of circuit integration in a single molded package to improve device reliability.

The IMCs formed during the annealing process consists of multiple metal compounds. The delamination or void growth occurs when the IMCs are under the thermal field[31]. Kim *et al.* studied the compositions of Cu–Al IMCs under annealing process by using the TEM technique[150]. It is founded that $CuAl_2$ (θ), CuAl (η_2) and Cu_9Al_4 (γ_2) are the main structures in the IMCs during the annealing process. The different structures of IMCs could be measured by using FFT patterns as shown in Figs. 8(d)–8(f). The delamination or void growth occurs are uneven on the Cu–Al surface shown in Fig. 8(g).

By studying the mechanism of WB microstructure evolution under the heating field, the nature of IMCs could be observed dynamically[34, 152–154]. The IMC mechanism was further studied by Xu *et al.*[36]. The process of IMCs growth and phase transition were *in situ* recorded in Fig. 8(h). The annealing process occurred in the chamber of TEM using a thermal sample holder, and the evolution of the bonding interfacial

structure could be dynamically observed. A bilayer of IMCs with $CuAl_2$ and Cu_9Al_4 formed. The $CuAl_2$ started transforming into CuAl when the Al pad was consumed greatly. With the continuous decrease of Al element, the CuAl layer and $CuAl_2$ transformed into Cu_9Al_4 under the annealing process as shown in Fig. 8(h). The final phase in IMC is the Cu_9Al_4.

Memory package is an important field in the semiconductor industry and its reliability greatly affects the device performance. More advanced electron microscopy will be used to study the package stability issues.

4. Conclusion

The NVMs characterized by the *in situ* TEM techniques combined with multiple stimuli such as e-beam, electrical field, heating field have been reviewed in this article. The switching mechanisms during the SET/RESET process have been discussed as well. From the above experiments and discussions, the future development directions, performance optimizations, characterization tools improvement and reliability research are all pointed out.

In the future, more advanced *in situ* experiments are needed, such as force or optical fields combined with TEM. As the continued scaling down memory devices, the high efficiency and the versatility of *in situ* TEM techniques are needed. The physical mechanism of the memory devices, such as the charge storage, DWs inverse, negative capacitance effect and so on[155–158]. The next generation TEM techniques should aim to provide a comprehensive analysis with higher spatial resolution and energy resolution[4, 159].

Here, we summarized the current applications and technical challenges for employing *in situ* TEM techniques on the mechanism study of NVMs as the following three aspects:

(1) The resolution of light element for TEM image should be improved[160–163]. For example, the *in situ* study in FeRAM requires the observation of oxygen atom displacement at a subtle scale. There is plenty of room to improve the spatial resolution combining various contrast principles such as increasing the acceleration voltage, adding an objective lens and the dyeing corresponding compositions.

(2) Advanced technical developments are needed about *in situ* TEM to observe the charge storage in the memory devices. The electronic holography method is an effective tool for imaging the electron potential distribution. A faster charge-coupled device (CCD) and big data technology are needed to record the process. The current time resolution of TEM equipped with CCD can reach a picosecond level[164, 165]. Faster CCD could improve TEM time resolution during the characterization of the switching process[166–168].

(3) EMCD is a powerful technique for the *in situ* studies of MRAM. The dynamic observation of magnetic domains could be implemented under a high time resolution[169–173].

The development of information technology has greatly promoted the memory storage density and speed[174–180]. Electron microscopy, especially the *in situ* TEM technology provides an opportunity to study the dynamic structural evolution to better understand the physical mechanism of the memory device.

Acknowledgements

This work is supported by the Projects of Science and Technology Commission of Shanghai Municipality (19ZR1473800 and 14DZ2260800), the Shanghai Rising-Star Program (17QA1401400), Young Elite Scientists Sponsorship Program by CAST (YESS), and the Fundamental Research Funds for the Central Universities.

References

[1] Luo C, Wang C L, Wu X, et al. *In situ* transmission electron microscopy characterization and manipulation of two-dimensional layered materials beyond graphene. Small, 2017, 13, 1604259

[2] Jiang Y, Chen Z, Han Y M, et al. Electron ptychography of 2D materials to deep sub-ångström resolution. Nature, 2018, 559, 343

[3] Xu H, Wu X, Tian X, et al. Dynamic structure-properties characterization and manipulation in advanced nanodevices. Mater Today Nano, 2019, 7, 100042

[4] Lanza M, Wong H S P, Pop E, et al. Recommended methods to study resistive switching devices. Adv Electron Mater, 2019, 5, 1800143

[5] Fan Z, Zhang L Q, Baumann D, et al. *In situ* transmission electron microscopy for energy materials and devices. Adv Mater, 2019, 31, 1900608

[6] Cao Y M, Zhang B, Tian X Y, et al. Direct covalent modification of black phosphorus quantum dots with conjugated polymers for information storage. Nanoscale, 2019, 11, 3527

[7] Endoh T, Koike H, Ikeda S, et al. An overview of nonvolatile emerging memories: Spintronics for working memories. IEEE J Emerg Sel Top Circuits Syst, 2016, 6, 109

[8] Zhang Z H, Wang Z W, Shi T, et al. Memory materials and devices: From concept to application. InfoMat, 2020, 2, 261

[9] Sun W, Gao B, Chi M F, et al. Understanding memristive switching via *in situ* characterization and device modeling. Nat Commun, 2019, 10, 3453

[10] Lee S H, Zhu X J, Lu W D. Nanoscale resistive switching devices for memory and computing applications. Nano Res, 2020, 13, 1228

[11] Zhang Y, Wang Z R, Zhu J D, et al. Brain-inspired computing with memristors: Challenges in devices, circuits, and systems. Appl Phys Rev, 2020, 7, 011308

[12] Wang Z P, Zhang S R, Zhou L, et al. Functional non-volatile memory devices: From fundamentals to photo-tunable properties. Phys Status Solidi RRL, 2019, 13, 1970022

[13] Younis A, Li S A. Microscopic investigations of switching phenomenon in memristive systems: A mini review. RSC Adv, 2018, 8, 28763

[14] Gao H, Yang Y X, Wang Y J, et al. Transparent, flexible, fatigue-free, optical-read, and nonvolatile ferroelectric memories. ACS Appl Mater Interfaces, 2019, 11, 35169

[15] Si M W, Saha A K, Gao S J, et al. A ferroelectric semiconductor field-effect transistor. Nat Electron, 2019, 2, 580

[16] Cao R R, Liu Q, Liu M, et al. Improvement of endurance in HZO-based ferroelectric capacitor using Ru electrode. IEEE Electron Device Lett, 2019, 40, 1744

[17] Chang T C, Chang K C, Tsai T M, et al. Resistance random access memory. Mater Today, 2016, 19, 254

[18] Wang H, Yan X B. Overview of resistive random access memory (RRAM): Materials, filament mechanisms, performance optimization, and prospects. Phys Status Solidi RRL, 2019, 13, 1900073

[19] Yen T J, Gismatulin A, Volodin V, et al. All nonmetal resistive random access memory. Sci Rep, 2019, 9, 6144

[20] Li W Q, Zhan X Y, Song X Y, et al. A review of recent applications of ion beam techniques on nanomaterial surface modification: Design of nanostructures and energy harvesting. Small, 2019, 15, 1901820

[21] Zhang W, Mazzarello R, Wuttig M, et al. Designing crystalliza-

tion in phase-change materials for universal memory and neuro-inspired computing. Nat Rev Mater, 2019, 4, 150
[22] Burr G W, Brightsky M J, Sebastian A, et al. Recent progress in phase-change_newline memory technology. IEEE J Emerg Sel Top Circuits Syst, 2016, 6, 146
[23] Jiang T T, Wang J J, Lu L, et al. Progressive amorphization of GeSbTe phase-change material under electron beam irradiation. APL Mater, 2019, 7, 081121
[24] Wang P F, Lin X, Liu L, et al. A semi-floating gate transistor for low-voltage ultrafast memory and sensing operation. Science, 2013, 341, 640
[25] Yao Y, Liu L, Ye Z Y, et al. Investigation of device physics and modeling of semi-floating gate image sensor cell. Microelectron Eng, 2019, 217, 111111
[26] Rathore J S, Fandan R, Srivastava S, et al. Self-assembled Sn nanocrystals as the floating gate of nonvolatile flash memory. ACS Appl Electron Mater, 2019, 1, 1852
[27] Yao Y, Li C, Huo Z L, et al. *In situ* electron holography study of charge distribution in high-κ charge-trapping memory. Nat Commun, 2013, 4, 2764
[28] Fernández-Pacheco A, Streubel R, Fruchart O, et al. Three-dimensional nanomagnetism. Nat Commun, 2017, 8, 15756
[29] Yakushiji K, Sugihara A, Nakano T, et al. Fully epitaxial magnetic tunnel junction on a silicon wafer. Appl Phys Lett, 2019, 115, 202403
[30] Stavrou V D, Kourounis D, Dimakopoulos K, et al. Magnetic skyrmions in FePt nanoparticles having Reuleaux 3D geometry: A micromagnetic simulation study. Nanoscale, 2019, 11, 20102
[31] Yang Z, Mi X J, Feng X, et al. Interface evolution of Cu–Ni–Si/Al–Mg–Si clad composite wires after annealing. Rare Met, 2018, 42, 1
[32] Moisy F, Sauvage X, Hug E. Investigation of the early stage of reactive interdiffusion in the Cu-Al system by *in situ* transmission electron microscopy. Materialia, 2020, 9, 100633
[33] Xu H, Liu C, Silberschmidt V V, et al. Behavior of aluminum oxide, intermetallics and voids in Cu–Al wire bonds. Acta Mater, 2011, 59, 5661
[34] Liu C P, Chang S J, Liu Y F, et al. Cu–Al interfacial formation and kinetic growth behavior during HTS reliability test. J Mater Process Technol, 2019, 267, 90
[35] Liu D, Chen H B, Wu J S, et al. Corrosion behavior of Cu–Al intermetallic compounds in copper wire bonding in chloride-containing accelerated humidity testing. 2016 IEEE 66th Electronic Components and Technology Conference (ECTC), 2016, 629
[36] Xu H, Qin I, Clauberg H, et al. New observation of nanoscale interfacial evolution in micro Cu–Al wire bonds by *in situ* high resolution TEM study. Scr Mater, 2016, 115, 1
[37] Tan Y Y, Yang Q L, Sim K S, et al. Cu–Al intermetallic compound investigation using ex-situ post annealing and *in situ* annealing. Microelectron Reliab, 2015, 55, 2316
[38] Wang C M. *In situ* transmission electron microscopy and spectroscopy studies of rechargeable batteries under dynamic operating conditions: A retrospective and perspective view. J Mater Res, 2015, 30, 326
[39] Legros M. *In situ* mechanical TEM: Seeing and measuring under stress with electrons. Comptes Rendus Physique, 2014, 15, 224
[40] Xiang B, Hwang D J, In J B, et al. *In situ* TEM near-field optical probing of nanoscale silicon crystallization. Nano Lett, 2012, 12, 2524
[41] Evans J E, Jungjohann K L, Browning N D, et al. Controlled growth of nanoparticles from solution with *in situ* liquid transmission electron microscopy. Nano Lett, 2011, 11, 2809
[42] Chernavskii P A, Pankina G V, Chernavskii A P, et al. *In situ* magnetic study of the low-temperature oxidation of carbon-supported cobalt nanoparticles. J Phys Chem C, 2007, 111, 5576
[43] Midgley P A, Dunin-Borkowski R E. Electron tomography and holography in materials science. Nat Mater, 2009, 8, 271
[44] Zweck J. Imaging of magnetic and electric fields by electron microscopy. J Phys: Condens Matter, 2016, 28, 403001
[45] Yang H, Li Y L, Zhu H L, et al. Advanced TEM application in 10nm below technology node device analysis. 2019 IEEE 26th International Symposium on Physical and Failure Analysis of Integrated Circuits (IPFA), 2019, 1
[46] Choi S J, Park G S, Kim K H, et al. *In situ* observation of voltage-induced multilevel resistive switching in solid electrolyte memory. Adv Mater, 2011, 23, 3272
[47] Cha D, Ahn S J, Park S Y, et al. A direct observation on the structure evolution of memory-switching phenomena using *in situ* TEM. 2009 Symposium on VLSI Technology, 2009, 204
[48] Martín G, González M B, Varea A, et al. Resistive switching studies of ReRAM devices by *in situ* TEM. Microsc Microanal, 2019, 25, 71
[49] Zhang J Y, Yu Y, Wang P, et al. Characterization of atomic defects on the photoluminescence in two-dimensional materials using transmission electron microscope. InfoMat, 2019, 1, 85
[50] Wu X, Pey K L, Zhang G, et al. Electrode material dependent breakdown and recovery in advanced high-κ gate stacks. Appl Phys Lett, 2010, 96, 202903
[51] Huang P, Zhang P, Xu S G, et al. Recent advances in two-dimensional ferromagnetism: Materials synthesis, physical properties and device applications. Nanoscale, 2020, 12, 2309
[52] Kim D H, Ning S, Ross C A. Self-assembled multiferroic perovskite–spinel nanocomposite thin films: Epitaxial growth, templating and integration on silicon. J Mater Chem C, 2019, 7, 9128
[53] Pan E, Bai G X, Lei L, et al. The electrical enhancement and reversible manipulation of near-infrared luminescence in Nd doped ferroelectric nanocomposites for optical switches. J Mater Chem C, 2019, 7, 4320
[54] Guo R, Wang Y, Yoong H Y, et al. Effect of extrinsically introduced passive interface layer on the performance of ferroelectric tunnel junctions. ACS Appl Mater Interfaces, 2017, 9, 5050
[55] Catalan G, Scott J F. Physics and applications of bismuth ferrite. Adv Mater, 2009, 21, 2463
[56] Chiu C H, Huang C W, Hsieh Y H, et al. *In-situ* TEM observation of multilevel storage behavior in low power FeRAM device. Nano Energy, 2017, 34, 103
[57] Li L Z, Britson J, Jokisaari J R, et al. Giant resistive switching via control of ferroelectric charged domain walls. Adv Mater, 2016, 28, 6574
[58] Wang Z Q, Zhong X Y, Yu R, et al. Quantitative experimental determination of site-specific magnetic structures by transmitted electrons. Nat Commun, 2013, 4, 1395
[59] Deng Y, Gammer C, Ciston J, et al. Atomic resolution probing of phase transformations and domain evolution during large superelastic deformation in ferroelectrics with *in situ* TEM. Microsc Microanal, 2019, 25, 1850
[60] Eerenstein W, Mathur N D, Scott J F. Multiferroic and magnetoelectric materials. Nature, 2006, 442, 759
[61] Li L Z, Zhang Y, Xie L, et al. Atomic-scale mechanisms of defect-induced retention failure in ferroelectrics. Nano Lett, 2017, 17, 3556
[62] Wu X, Yu K H, Cha D, et al. Atomic scale modulation of self-rectifying resistive switching by interfacial defects. Adv Sci, 2018, 5, 1800096
[63] Auciello O, Scott J F, Ramesh R. The physics of ferroelectric memories. Phys Today, 1998, 51, 22
[64] Zhang Y Y, Han M G, Garlow J A, et al. Deterministic ferroelastic domain switching using ferroelectric bilayers. Nano Lett, 2019, 19, 5319
[65] Tan A J, Zhu Z W, Choe H S, et al. Ferroelectric Si-doped HfO_2 capacitors for next-generation memories. 2019 International Symposium on VLSI Technology, Systems and Application (VLSI-

TSA), 2019, 1
[66] Molinari A, Witte R, Neelisetty K K, et al. Configurable resistive response in $BaTiO_3$ ferroelectric memristors via electron beam radiation. Adv Mater, 2020, 32, 1907541
[67] Yoon J S, Tewari A, Shin C, et al. Influence of high-pressure annealing on memory properties of $Hf_{0.5}Zr_{0.5}O_2$ based 1T-FeRAM. IEEE Electron Device Lett, 2019, 40, 1076
[68] Lee J H, Wu C, Sung S, et al. Highly flexible and stable resistive switching devices based on WS_2 nanosheets: Poly(methylmethacrylate) nanocomposites. Sci Rep, 2019, 9, 19316
[69] Chen Y C, Lin C C, Hu S T, et al. A novel resistive switching identification method through relaxation characteristics for sneak-path-constrained selectorless RRAM application. Sci Rep, 2019, 9, 12420
[70] Mei S, Bosman M, Shubhakar K, et al. 3D characterization of hard breakdown in RRAM device. Microelectron Eng, 2019, 216, 111042
[71] Zhang L, Zhu L, Li X M, et al. Resistive switching mechanism in the one diode-one resistor memory based on p^+-Si/n-ZnO heterostructure revealed by *in situ* TEM. Sci Rep, 2017, 7, 45143
[72] Qiu J T, Samanta S, Dutta M, et al. Controlling resistive switching by using an optimized MoS_2 interfacial layer and the role of top electrodes on ascorbic acid sensing in TaO_x-based RRAM. Langmuir, 2019, 35, 3897
[73] Gan K J, Liu P T, Chien T C, et al. Highly durable and flexible gallium-based oxide conductive-bridging random access memory. Sci Rep, 2019, 9, 14141
[74] Jiang H, Han L L, Lin P, et al. Sub-10 nm Ta channel responsible for superior performance of a HfO_2 memristor. Sci Rep, 2016, 6, 28525
[75] Li C, Gao B, Yao Y, et al. Memory devices: Direct observations of nanofilament evolution in switching processes in HfO_2-based resistive random access memory by *in situ* TEM studies. Adv Mater, 2017, 29, 1602976
[76] Li X, Tung C H, Pey K L. The nature of dielectric breakdown. Appl Phys Lett, 2008, 93, 072903
[77] Liu Q, Sun J, Lv H, et al. Real-time observation on dynamic growth/dissolution of conductive filaments in oxide-electrolyte-based ReRAM. Adv Mater, 2012, 24, 1844
[78] Zintler A, Eilhardt R, Petzold S, et al. Correlation of structural modifications by multiscale phase mapping in filamentary type HfO_2-based RRAM: Towards a component specific *in situ* TEM investigation. Microsc Microanal, 2019, 25, 1842
[79] Lu X, Adkins E R, He Y, et al. Germanium as a sodium ion battery material: In situ TEM reveals fast sodiation kinetics with high capacity. Chem Mater, 2016, 28, 1236
[80] Zhu Y B, Zheng K, Wu X, et al. Enhanced stability of filament-type resistive switching by interface engineering. Sci Rep, 2017, 7, 43664
[81] Wu X, Mei S, Bosman M, et al. Evolution of filament formation in $Ni/HfO_2/SiO_x/Si$-based RRAM devices. Adv Electron Mater, 2015, 1, 1500130
[82] Pey K L, Thamankar R, Sen M, et al. Understanding the switching mechanism in RRAM using *in situ* TEM. 2016 IEEE Silicon Nanoelectron Work, 2016, 36
[83] Yang Y C, Gao P, Li L Z, et al. Electrochemical dynamics of nanoscale metallic inclusions in dielectrics. Nat Commun, 2014, 5, 4232
[84] Tian X Z, Wang L F, Wei J K, et al. Filament growth dynamics in solid electrolyte-based resistive memories revealed by *in situ* TEM. Nano Res, 2014, 7, 1065
[85] Chen J Y, Hsin C L, Huang C W, et al. Dynamic evolution of conducting nanofilament in resistive switching memories. Nano Lett, 2013, 13, 3671
[86] Zhang F, Zhang H R, Krylyuk S, et al. Electric-field induced structural transition in vertical $MoTe_2$- and $Mo_{1-x}W_xTe_2$-based resistive memories. Nat Mater, 2019, 18, 55
[87] Lee J, Schell W, Zhu X J, et al. Charge transition of oxygen vacancies during resistive switching in oxide-based RRAM. ACS Appl Mater Interfaces, 2019, 11, 11579
[88] Yang Y C, Zhang X X, Qin L, et al. Probing nanoscale oxygen ion motion in memristive systems. Nat Commun, 2017, 8, 15173
[89] Sivan M, Li Y, Veluri H, et al. All WSe_2 1T1R resistive RAM cell for future monolithic 3D embedded memory integration. Nat Commun, 2019, 10, 5201
[90] Sun C, Lu S M, Jin F, et al. Multi-factors induced evolution of resistive switching properties for $TiN/Gd_2O_3/Au$ RRAM devices. J Alloy Compd, 2020, 816, 152564
[91] Yang R, Li H, Smithe K K H, et al. Ternary content-addressable memory with MoS_2 transistors for massively parallel data search. Nat Electron, 2019, 2, 108
[92] Li L, Chang K C, Ye C, et al. An indirect way to achieve comprehensive performance improvement of resistive memory: When hafnium meets ITO in an electrode. Nanoscale, 2020, 12, 3267
[93] Bersuker G, Gilmer D C, Veksler D. Metal-oxide resistive random access memory (RRAM) technology: Material and operation details and ramifications. In: Advances in Non-Volatile Memory and Storage Technology. Amsterdam: Elsevier, 2019, 35
[94] Dash C S, Prabaharan S R S. Nano resistive memory (Re-RAM) devices and their applications. Rev Adv Mater Sci, 2019, 58, 248
[95] Li Q L, Zhang J Y, Li Q H, et al. Review of printed electrodes for flexible devices. Front Mater, 2019, 5, 77
[96] Bi H C, Wan S, Cao X H, et al. A general and facile method for preparation of large-scale reduced graphene oxide films with controlled structures. Carbon, 2019, 143, 162
[97] Pries J, Wei S, Wuttig M, et al. Switching between crystallization from the glassy and the undercooled liquid phase in phase change material $Ge_2Sb_2Te_5$. Adv Mater, 2019, 31, 1900784
[98] Chen B, Chen Y M, Ding K Y, et al. Kinetics features conducive to cache-type nonvolatile phase-change memory. Chem Mater, 2019, 31, 8794
[99] Lotnyk A, Behrens M, Rauschenbach B. Phase change thin films for non-volatile memory applications. Nanoscale Adv, 2019, 1, 3836
[100] Raoux S, Xiong F, Wuttig M, et al. Phase change materials and phase change memory. MRS Bull, 2014, 39, 703
[101] Wang Y, Guo T Q, Liu G Y, et al. Sc-centered octahedron enables high-speed phase change memory with improved data retention and reduced power consumption. ACS Appl Mater Interfaces, 2019, 11, 10848
[102] Meister S, Kim S, Cha J J, et al. *In situ* transmission electron microscopy observation of nanostructural changes in phase-change memory. ACS Nano, 2011, 5, 2742
[103] Shen X, Chen Y M, Wang G X, et al. Phase-change memory and optical data storage. Springer Handbook of Glass. Cham: Springer International Publishing, 2019, 1495
[104] Durai S, Raj S, Manivannan A. An extremely fast, energy-efficient RESET process in $Ge_2Sb_2Te_5$ phase change memory device revealed by the choice of electrode materials and interface effects. Semicond Sci Technol, 2020, 35, 015022
[105] Zhai F X, Yunqi H, Liu N N, et al. Bipolar resistive switching of $Ge_2Sb_2Te_5$ material. Proc SPIE 11209, Eleventh International Conference on Information Optics and Photonics (CIOP 2019), 2019, 1120, 1120939
[106] Yoo S, Eom T, Gwon T, et al. Bipolar resistive switching behavior of an amorphous $Ge_2Sb_2Te_5$ thin films with a Te layer. Nanoscale, 2015, 7, 6340
[107] Behrens M, Lotnyk A, Gerlach J W, et al. Direct measurement of crystal growth velocity in epitaxial phase-change material thin films. ACS Appl Mater Interfaces, 2019, 11, 41544
[108] Liu B H, Teo H W, Mo Z H, et al. *In situ* TEM study of electron-beam radiation induced boron diffusion and effects on phase

and microstructure evolution in nanostructured CoFeB/SiO_2 thin film. J Appl Phys, 2017, 121, 015111
[109] Son S, Jeon S, Oh J, et al. In-situ characterization of switching mechanisms in phase change random access memory (PRAM) using transmission electron microscopy (TEM). IEEE International Symposium for Testing and Failure Analysis, 2013, 236
[110] Kim T H, Ouyang G, Poplawsky J D, et al. *In-situ* TEM analysis of the phase transformation mechanism of a Cu–Al–Ni shape memory alloy. J Alloy Compd, 2019, 808, 151743
[111] Yu K H, Xu T, Wu X, et al. *In situ* observation of crystalline silicon growth from SiO_2 at atomic scale. Research, 2019, 2019, 1
[112] Ren K, Cheng Y, Xia M J, et al. *In-situ* observation of $Ge_2Sb_2Te_5$ crystallization at the passivated interface. Ceram Int, 2019, 45, 19542
[113] Zhu M, Song W X, Konze P M, et al. Direct atomic insight into the role of dopants in phase-change materials. Nat Commun, 2019, 10, 3525
[114] Bartlett P, Berg A I, Bernasconi M, et al. Phase-change memories (PCM) – Experiments and modelling: General discussion. Faraday Discuss, 2019, 213, 393
[115] Rao F, Zhang W, Ma E. Catching structural transitions in liquids. Science, 2019, 364, 1032
[116] Longo M. Advances in nanowire PCM. In: Advances in non-volatile memory and storage Technology. Amsterdam: Elsevier, 2019, 443
[117] Lee J, Choi S, Lee C, et al. GeSbTe deposition for the PRAM application. Appl Surf Sci, 2007, 253, 3969
[118] Zhang S M, Xu H, Liao F Y, et al. Wafer-scale transferred multilayer MoS_2 for high performance field effect transistors. Nanotechnology, 2019, 30, 174002
[119] Zhao L, Guo Z X, Wei Q L, et al. The relationship between the dislocations and microstructure in $In_{0.82}Ga_{0.18}As$/InP heterostructures. Sci Rep, 2016, 6, 35139
[120] Vu Q A, Shin Y S, Kim Y R, et al. Two-terminal floating-gate memory with van der Waals heterostructures for ultrahigh on/off ratio. Nat Commun, 2016, 7, 12725
[121] Hu D B, Zhang G C, Yang H H, et al. High-performance nonvolatile organic transistor memory using quantum dots-based floating gate. IEEE Trans Electron Devices, 2017, 64, 3816
[122] Kim S M, Song E B, Lee S, et al. Transparent and flexible graphene charge-trap memory. ACS Nano, 2012, 6, 7879
[123] Li Chao, Yao Yuan, Yang Yang, et al. *In situ* transmission electron microscopy studies on nanomaterials and HfO_2-based storage nanodevices. Acta Phys Sin, 2018, 67, 124
[124] Boureau V, Sklenard B, McLeod R, et al. Quantitative mapping of the charge density in a monolayer of MoS_2 at atomic resolution by off-axis electron holography. ACS Nano, 2020, 14, 524
[125] McCartney M R, Dunin-Borkowski R E, Smith D J. Quantitative measurement of nanoscale electrostatic potentials and charges using off-axis electron holography: Developments and opportunities. Ultramicroscopy, 2019, 203, 105
[126] Miyagawa H, Kusai H, Takaishi R, et al. Metal-assisted solid-phase crystallization process for vertical monocrystalline Si channel in 3D flash memory. 2019 IEEE International Electron Devices Meeting (IEDM), 2019, 28.3.1
[127] Verbeeck J, Tian H, Schattschneider P. Production and application of electron vortex beams. Nature, 2010, 467, 301
[128] Wang Z C, Tavabi A H, Jin L, et al. Atomic scale imaging of magnetic circular dichroism by achromatic electron microscopy. Nat Mater, 2018, 17, 221
[129] Wang Z C, Zhong X Y, Jin L, et al. Effects of dynamic diffraction conditions on magnetic parameter determination in a double perovskite Sr_2FeMoO_6 using electron energy-loss magnetic chiral dichroism. Ultramicroscopy, 2017, 176, 212
[130] Muto S, Rusz J, Tatsumi K, et al. Quantitative characterization of nanoscale polycrystalline magnets with electron magnetic circular dichroism. Nat Commun, 2014, 5, 3138
[131] Kronast F, Friedenberger N, Ollefs K, et al. Element-specific magnetic hysteresis of individual 18 nm Fe nanocubes. Nano Lett, 2011, 11, 1710
[132] Béché A, van Boxem R, van Tendeloo G, et al. Magnetic monopole field exposed by electrons. Nat Phys, 2014, 10, 26
[133] Iwata-Harms J M, Jan G, Serrano-Guisan S, et al. Ultrathin perpendicular magnetic anisotropy CoFeB free layers for highly efficient, high speed writing in spin-transfer-torque magnetic random access memory. Sci Rep, 2019, 9, 19407
[134] Jena A K, Satapathy S, Mohanty J. Magnetic properties and oxygen migration induced resistive switching effect in Y substituted multiferroic bismuth ferrite. Phys Chem Chem Phys, 2019, 21, 15854
[135] Rusz J, Muto S, Spiegelberg J, et al. Magnetic measurements with atomic-plane resolution. Nat Commun, 2016, 7, 12672
[136] Smirnov E, Sedoykina T, Orlov A, et al. Evaluation of a new MgO barrier based on CoFeB/MgO/CoFeB structure for advanced MRAM applications. Microelectron Eng, 2017, 167, 6
[137] Zhang Z H, Wang X F, Xu J B, et al. Evidence of intrinsic ferromagnetism in individual dilute magnetic semiconducting nanostructures. Nat Nanotech, 2009, 4, 523
[138] Lee G W, Ok E, Heo S, et al. Innovative approaches to the invisible defect on STT-MRAM. Microelectron Reliab, 2019, 100/101, 113431
[139] Jin S, McCormack M, Tiefel T H, et al. Colossal magnetoresistance in La–Ca–Mn–O ferromagnetic thin films. J Appl Phys, 1994, 76, 6929
[140] Zhu L J, Zhu L J, Shi S J, et al. Energy-efficient ultrafast SOT-MRAMs based on low-resistivity spin hall metal $Au_{0.25}Pt_{0.75}$. Adv Electron Mater, 2000, 6, 1901131
[141] Jackson E, Wu Y, Frost W, et al. Non-destructive imaging for quality assurance of magnetoresistive random-access memory junctions. J Phys D, 2019, 53, 014004
[142] Rusz J, Rubino S, Schattschneider P. First-principles theory of chiral dichroism in electron microscopy applied to 3d ferromagnets. Phys Rev B, 2007, 75, 214425
[143] Ali H S, Warnatz T, Xie L, et al. Quantitative EMCD by use of a double aperture for simultaneous acquisition of EELS. Ultramicroscopy, 2019, 196, 192
[144] Spiegelberg J, Song D S, Dunin-Borkowski R E, et al. Blind identification of magnetic signals in electron magnetic chiral dichroism using independent component analysis. Ultramicroscopy, 2018, 195, 129
[145] Ali H S, Warnatz T, Xie L, et al. Towards quantitative nanomagnetism in transmission electron microscope by the use of patterned apertures. Microsc Microanal, 2019, 25, 654
[146] Warot-Fonrose B, Houdellier F, Hÿtch M J, et al. Mapping inelastic intensities in diffraction patterns of magnetic samples using the energy spectrum imaging technique. Ultramicroscopy, 2008, 108, 393
[147] Krautscheid P, Reeve R M, Lauf M, et al. Domain wall spin structures in mesoscopic Fe rings probed by high resolution SEMPA. J Phys D, 2016, 49, 425004
[148] Gallagher W J, Chien E, Chiang T W, et al. Recent progress and next directions for embedded MRAM technology. 2019 Symposium on VLSI Circuits, 2019, T190
[149] Ikegawa S, Mancoff F B, Janesky J, et al. Magnetoresistive random access memory: Present and future. IEEE Trans Electron Devices, 2020, 67, 1407
[150] Kim H J, Lee J Y, Paik K W, et al. Effects of Cu/Al intermetallic compound (IMC) on copper wire and aluminum pad bondability. IEEE Trans Comp Packag Technol, 2003, 26, 367
[151] Reisner R, Liang S X, Pettyweeks S L, et al. Integrated passive cap in a system-in-package. Google Patents, 20080217708, 2008
[152] Qin W T, Anderson H, Anderson T, et al. Corrosion mechanisms

of Cu wire bonding on Al pads. 2018 IEEE 68th Electronic Components and Technology Conference (ECTC), 2018, 1446

[153] Lall P, Deshpande S, Nguyen L, et al. Microstructural indicators for prognostication of copper–aluminum wire bond reliability under high-temperature storage and temperature humidity. IEEE Trans Compon Packag Manuf Technol, 2016, 6, 569

[154] Mishler M, Ouvarov-Bancalero V, Chae S H, et al. Intermetallic compound growth and stress development in Al–Cu diffusion couple. J Electron Materi, 2018, 47, 855

[155] Wang C L, Wu X, Ma Y H, et al. Metallic few-layered VSe_2 nanosheets: High two-dimensional conductivity for flexible in-plane solid-state supercapacitors. J Mater Chem A, 2018, 6, 8299

[156] Wang C L, Wu X, Xu H J, et al. VSe_2/carbon-nanotube compound for all solid-state flexible in-plane supercapacitor. Appl Phys Lett, 2019, 114, 023902

[157] Long M, Wang Y, Wang P, et al. Palladium diselenide long-wavelength infrared photodetector with high sensitivity and stability. ACS Nano, 2019, 13, 2511

[158] Liang F, Xu H J, Dong Z Y, et al. Substrates and interlayer coupling effects on $Mo_{1-x}W_xSe_2$ alloys. J Semicond, 2019, 40, 062005

[159] Li J, Johnson G, Zhang S, et al. *In situ* transmission electron microscopy for energy applications. Joule, 2019, 3, 4

[160] Ross F M, Minor A M. In situ transmission electron microscopy. Springer Handbook of Microscopy. Cham: Springer International Publishing, 2019, 101

[161] Wu F, Li Q, Wang P, et al. High efficiency and fast van der Waals hetero-photodiodes with a unilateral depletion region. Nat Commun, 2019, 10, 4663

[162] Luo C, Yu K H, Wu X, et al. *In situ* interfacial manipulation of metastable states between nucleation and decomposition of single bismuth nanoparticle. Phys Status Solidi B, 2019, 256, 1970016

[163] Wu X, Luo C, Hao P, et al. Interfacial defects: Probing and manipulating the interfacial defects of InGaAs dual-layer metal oxides at the atomic scale. Adv Mater, 2018, 30, 1870013

[164] Barwick B, Park H S, Kwon O H, et al. 4D imaging of transient structures and morphologies in ultrafast electron microscopy. Science, 2008, 322, 1227

[165] Fu X W, Chen B, Tang J, et al. Imaging rotational dynamics of nanoparticles in liquid by 4D electron microscopy. Science, 2017, 355, 494

[166] Yang G L, Han W H, Xie T M, et al. Electronic holographic three-dimensional display with enlarged viewing angle using non-mechanical scanning technology. OSA Continuum, 2019, 2, 1917

[167] Wang M K, Liu J J, Ding Q L, et al. *In-situ* studies of magnetostriction in $Tb_xHo_{1-x}Fe_{1.9}Mn_{0.1}$ Laves compounds. J Magn Magn Mater, 2020, 501, 166422

[168] McCartney M R, Smith D J. Electron holography: Phase imaging with nanometer resolution. Ann Rev Mater Res, 2007, 37, 729

[169] Lidbaum H, Rusz J, Rubino S, et al. Reciprocal and real space maps for EMCD experiments. Ultramicroscopy, 2010, 110, 1380

[170] Zhong X Y. Atomic-plane resolved electron magnetic circular dichroism by achromatic spatially-resolved electron energy loss spectroscopy. Microsc Microanal, 2019, 25, 572

[171] Pohl D, Schneider S, Rusz J, et al. Electron vortex beams prepared by a spiral aperture with the goal to measure EMCD on ferromagnetic films via STEM. Ultramicroscopy, 2015, 150, 16

[172] Schattschneider P, Rubino S, Hébert C, et al. Detection of magnetic circular dichroism using a transmission electron microscope. Nature, 2006, 441, 486

[173] Negi D, Zeiger P M, Jones L, et al. Prospect for detecting magnetism of a single impurity atom using electron magnetic chiral dichroism. Phys Rev B, 2019, 100, 104434

[174] Luo Z W, Hu X T, Tian X Y, et al. Structure-property relationships in graphene-based strain and pressure sensors for potential artificial intelligence applications. Sensors, 2019, 19, 1250

[175] Tian X Y, Liu Z, Chu J H, et al. Dual-mode sensor and actuator to learn human-hand tracking and grasping. IEEE Trans Electron Devices, 2019, 66, 5407

[176] Liu S B, Wu X, Zhang D D, et al. Ultrafast dynamic pressure sensors based on graphene hybrid structure. ACS Appl Mater Interfaces, 2017, 9, 24148

[177] Xu H J, Wu X, Li X M, et al. Properties of graphene-metal contacts probed by Raman spectroscopy. Carbon, 2018, 127, 491

[178] Luo Z W, Li X M, Li Q L, et al. *In situ* dynamic manipulation of graphene strain sensor with drastically sensing performance enhancement. Adv Electron Mater, 2020, 6, 2000269

[179] Wang C L, Wu X, Zhang X, et al. Iron-doped VSe_2 nanosheets for enhanced hydrogen evolution reaction. Appl Phys Lett, 2020, 116, 223901

[180] Luo C, Li J F, Yang X, et al. *In situ* interfacial sublimation of Zn_2GeO_4 nanowire for atomic-scale manufacturing. ACS Appl Nano Mater, 2020, 3, 4747

Xin Yang got her BS from Nantong University in 2019. Now she is a MS student at East China Normal University under the supervision of Prof. Xing Wu. Her research focuses on *in situ* TEM study on the reliability of traditional semiconductor devices.

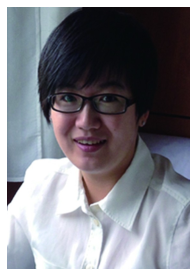

Xing Wu got her BS degree in 2008 at Xi'an Jiaotong University and PhD degree in 2012 at Nanyang Technological University. Then she worked at the Singapore University of Design and Technology and Southeast University. In 2014, she joined East China Normal University as a full professor. Her research interests include *in situ* TEM characterization of nano-devices.

Junhao Chu got his BS degree in 1966 at Shanghai Normal University China, and master's and PhD degrees from the Shanghai Institute of Technical Physics, Chinese Academy of Sciences (CAS) China in 1981 and 1984, respectively. From 1986 to 1988, he was a Humboldt Fellow at the Technical University of Munich, Germany. From 1993 to 2003 he was Director of the National Laboratory for Infrared Physics. He is currently a professor at East China Normal University and the Shanghai Institute of Technical Physics of the CAS and a member of the CAS. His research interests include semiconductor physics and device technology.